Electrodynamical Light Trapping Using Whispering-Gallery Resonances in Hyperbolic Cavities

Chihhui Wu,[1] Alessandro Salandrino,[1] Xingjie Ni,[1] and Xiang Zhang[1,2,*]

[1]*Nanoscale Science and Engineering Center, 5130 Etcheverry Hall, University of California, Berkeley, California 94720-1740, USA*

[2]*Materials Science Division, Lawrence Berkeley National Laboratory, 1 Cyclotron Road, Berkeley, California 94720, USA*

(Received 6 October 2013; revised manuscript received 12 February 2014; published 22 April 2014)

We theoretically study spherical cavities composed of hyperbolic metamaterials with indefinite permittivity tensors. Such cavities are capable of electrodynamically confining fields with deep subwavelength cavity sizes. The supported resonant modes are analogous to the whispering-gallery modes found in dielectric microcavities with much larger physical sizes. Because of the nature of electrodynamical confinement, these hyperbolic metamaterial cavities exhibit quality factors higher than predicted in the electrostatic limit. In addition, confining electromagnetic fields into the small cavities results in an extremely high photonic local density of states.

DOI: 10.1103/PhysRevX.4.021015 Subject Areas: Optics, Plasmonics

Manipulating electromagnetic waves with engineered structures leads to strongly modified light-matter interactions, which in turn affect various interesting phenomena in areas such as quantum optics [1] and nonlinear light generation [2]. Strong confinement of light using photonic or plasmonic structures has found applications ranging from the enhanced efficiency of light emitters [3–6], optical modulation [7,8], and molecule sensing [9] to energy harvesting [10,11]. In particular, localized surface-plasmon polaritons (LSPPs) supported by metallic nanoparticles are capable of trapping light even when the particle sizes are much smaller than the natural resonance wavelengths, giving rise to strong electromagnetic field confinement [12–14]. Such confined resonant modes are described as electrostatic resonances, in which case light is mostly stored in the form of electric energy [15]. Although one can, in principle, achieve ultrasmall mode volume by using LSPP resonators, the electrostatic nature of such resonators limits the quality factor of the resonances because induced displacement currents inside metals generate intrinsic Ohmic loss.

On the other hand, microcavities and photonic crystals confine light in an electrodynamical manner, in which case half of the stored energy is electric energy and the other is magnetic energy. Unlike LSPP resonators, these cavities have little Ohmic loss associated with the constituting materials. By using microspheres and toroids, the whispering-gallery modes (WGMs) exhibit quality factors as high as 10^9 [16,17]. Nevertheless, the physical size of such a cavity is typically much larger than the wavelength, i.e., $D \gg \lambda/n$, where D is the cavity size, λ is the natural resonance wavelength, and n is the optical index of the material. Large cavity size, in general, limits the achievable local field enhancement.

Indefinite media, also known as hyperbolic metamaterials (HMMs), exhibit unusual hyperbolic dispersion because of anisotropic permittivity of opposite signs along different directions [18]. Microcavities made of HMMs have been shown to support Fabry-Perot-type resonances with effective refractive indices as high as 17.4 [19]. Such hyperbolic cavities exhibit deep subwavelength confinement of electromagnetic waves due to the large effective indices. In this paper, we theoretically study the WGMs supported by spherical cavities composed of hyperbolic metamaterials. Compared to the previously demonstrated Fabry-Perot resonances that are due to effectively high optical indices, the WGMs to be studied here are caused by the indefinite nature of the permittivity tensors, as will be shown in the following. Differently from the LSPP resonances that also confine light within subwavelength regions, we show that light can be electrodynamically trapped by the WGMs of the hyperbolic spherical cavities. Such electrodynamical confinement of light leads to less electric energy stored inside the metal, and therefore less Ohmic damping and higher Q factors associated with the resonant modes.

The schematic of the spherical cavity is illustrated in Fig. 1(a). It is constituted of alternating metal and dielectric layers, with the thickness of each pair (denoted as a functional pair in the following discussion) being d. The filling ratio f of the metallic region is defined such that the metal thickness is $f \cdot d$ and the dielectric thickness is $(1-f) \cdot d$. Although f is an important parameter that

*xzhang@me.berkeley.edu

controls various optical properties of the cavities, the underlying physics to be discussed remains similar regardless of the choice of f. For simplicity, we keep $f = 0.5$ in the following discussion unless otherwise specified. We consider silver as the metal layers, and for its permittivity, we use the Drude model $\epsilon_{\mathrm{Ag}} = \epsilon_\infty - \omega_p^2/[\omega(\omega + i\omega_c)]$, with $\epsilon_\infty = 3.8355$, $\omega_p = 1.3937 \times 10^{16}$ rad/s, and $\omega_c = 2.9588 \times 10^{13}$ rad/s. The parameters of the Drude model are obtained by fitting the experimentally measured data from Ref. [20] at the wavelengths ranging from 750 to 1900 nm. The dielectric is assumed a permittivity of $\epsilon_d = 2.25$.

Under the effective medium description, the permittivity tensor of the hyperbolic medium takes the form

$$\bar{\epsilon} = \hat{r}\,\hat{r}\,\epsilon_r + \hat{\theta}\,\hat{\theta}\,\epsilon_t + \hat{\phi}\,\hat{\phi}\,\epsilon_t. \tag{1}$$

In the following, we consider $\epsilon_r = \epsilon_{\mathrm{Ag}}\epsilon_d/((1-f)\epsilon_{\mathrm{Ag}} + f\epsilon_d) > 0$ and $\epsilon_t = f\epsilon_{\mathrm{Ag}} + (1-f)\epsilon_d < 0$ inside the hyperbolic medium, while $\epsilon_r = \epsilon_t = 1$ elsewhere. The hyperbolic isofrequency contour of the hyperbolic medium is shown in Fig. 1(b) as an example. In the spherical cavity,

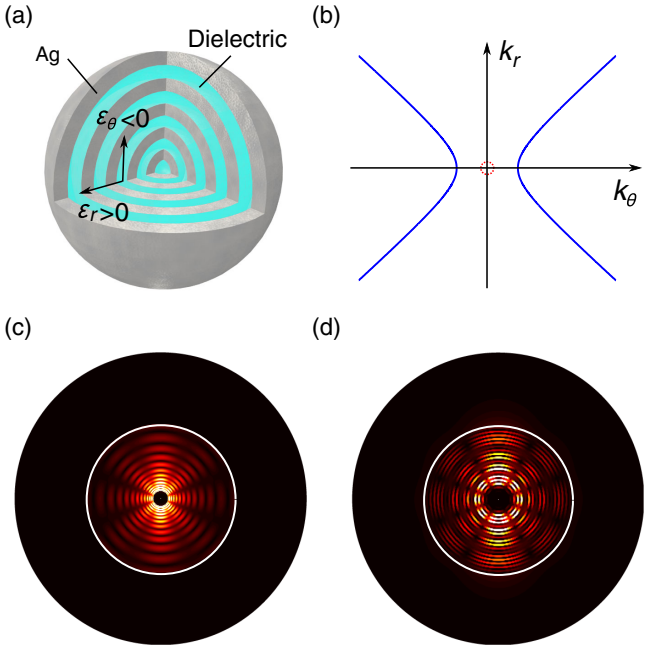

FIG. 1. (a) A schematic of the hyperbolic cavity composed of alternating metal and dielectric layers. (b) The isofrequency contour (solid line) in the momentum space calculated with the effective medium approximation with $\lambda = 1000$ nm. The small dotted circle at the center represents the isofrequency contour in vacuum at the same wavelength. A whispering-gallery resonance supported by (c) a homogeneous hyperbolic cavity and (d) a multilayer structure with $l = 4$. The cavity in (c) has an inner radius of 20 nm and an outer radius of 200 nm, with the resonant wavelength being $\lambda = 992$ nm. The cavity in (d) is composed of 20 functional layers with a thickness of 10 nm for each. The resonant wavelength in (d) is $\lambda = 977$ nm.

we include an empty void at the center of the cavity to avoid an ill-defined permittivity tensor at $r = 0$. The inner radius of the cavity is defined as R_c, and the outer radius is R. By using the vector spherical harmonics, one can express the electric field according to [21,22]

$$\begin{aligned}
\vec{E}^{(l)}(r < R_c) &= c_0 \vec{N}^{(1)}_{l,m}(k_0\vec{r}),\\
\vec{E}^{(l)}(R_c \le r < R) &= c_1 \vec{N}^{(1)}_{g(l),m}(k_t\vec{r}) + c_2 \vec{N}^{(2)}_{g(l),m}(k_t\vec{r}),\\
\vec{E}^{(l)}(R \le r) &= c_3 \vec{N}^{(3)}_{l,m}(k_0\vec{r})
\end{aligned} \tag{2}$$

and

$$\begin{aligned}
\vec{N}^{(p)}_{l,m}(\vec{x}) = {}& \frac{1}{x}\frac{d}{dx}[\sqrt{x} Z^{(p)}_{l+(1/2)}(x)]\vec{V}^{(3)}_{l,m}(\hat{x})\\
&+ \frac{\sqrt{l(l+1)}}{x^{3/2}} Z^{(p)}_{l+(1/2)}(x)\vec{V}^{(1)}_{l,m}(\hat{x}),
\end{aligned} \tag{3}$$

$$\begin{aligned}
\vec{N}^{(p)}_{g(l),m}(\vec{x}) = {}& \frac{1}{x}\frac{d}{dx}[\sqrt{x} Z^{(p)}_{g(l)+(1/2)}(x)]\vec{V}^{(3)}_{l,m}(\hat{x})/\epsilon_t\\
&+ \frac{\sqrt{l(l+1)}}{x^{3/2}} Z^{(p)}_{g(l)+(1/2)}(x)\vec{V}^{(1)}_{l,m}(\hat{x})/\epsilon_r.
\end{aligned} \tag{4}$$

$\vec{x} = x\hat{x}$, and $Z^{(p)}_{l+(1/2)}(x)$ is the Bessel function of the pth kind with the order being $l + \frac{1}{2}$. $\vec{V}^{(1)}_{l,m}(\hat{x})$ and $\vec{V}^{(3)}_{l,m}(\hat{x})$ are the vector spherical harmonics. Notice that inside the hyperbolic medium with the permittivity given by Eq. (1), the order of the Bessel function is not a half-integer, but instead

$$g(l) + \frac{1}{2} = \frac{1}{2}\sqrt{1 + \frac{4l(l+1)\epsilon_t}{\epsilon_r}}. \tag{5}$$

Interestingly, when the permittivity tensor is anisotropic and indefinite, such that $1 + (4l(l+1)\epsilon_t)/\epsilon_r < 0$, the order of the Bessel function becomes imaginary. The asymptotic behaviors of the two linearly independent Bessel functions with complex orders $g(l) + \frac{1}{2} = i\nu$ are given by $Z^{(1),(2)}_{i\nu}(x) \approx \cos[\nu \log(x)]$ and $\sin[\nu \log(x)]$, which are distinctive from the Bessel functions with real orders. In the limit of subwavelength cavity size ($\sqrt{\epsilon_t}k_0 R \ll 1$), we can use the asymptotic expression to find the resonance condition

$$\tan\left[\nu \log\left(\frac{R}{R_c}\right)\right] = \frac{(2l+1)\epsilon_T^{-1}\nu}{[\frac{1}{2}\epsilon_T^{-1} - (l+1)][\frac{1}{2}\epsilon_T^{-1} + l] + (\epsilon_T^{-1}\nu)^2}, \tag{6}$$

where $\nu = -i[g(l) + \frac{1}{2}] = \frac{1}{2}\sqrt{(-4l(l+1)\epsilon_t/\epsilon_r) - 1}$ increases with the wavelength. Since the tangent function on the left-hand side oscillates between $-\infty$ and ∞ with increasing ν while the right-hand side stays finite, Eq. (6) implies that

the hyperbolic cavities support WGMs with no cutoff frequencies even with deep subwavelength cavity sizes.

In the multilayer implement of the hyperbolic medium shown in Fig. 1(a), the achievable resonant wavelength is not arbitrarily long and depends on the number of functional pairs constituting the hyperbolic cavity. The reason for the cutoff of the resonant wavelengths is because the variation of the E field increases toward the center of the cavity, and the effective medium description eventually breaks down when the variation of the E field across one functional pair is large, i.e., $|\frac{d}{dr}E_r/E_r| > 1/d$. By increasing the number of functional pairs, the multilayer cavity can be better described as an effective medium and therefore supports WGMs with longer resonant wavelengths. We calculate the resonant modes of the multilayer structure by using the Mie theory [21]. The relation between the maximum resonant wavelengths and the number of functional pairs is given in Fig. 2(a), with the radius of the cavity fixed at 100 nm. The electric and magnetic fields inside each layer are expanded using vector spherical harmonics, and the scattering matrix is obtained by matching the boundary conditions at the interfaces between constituting layers. The eigenfrequencies of the resonant modes are obtained from the singularities of the scattering matrix in the complex frequency plane.

The deep subwavelength size of the cavity results in an extremely high radiative quality factor $Q_{\mathrm{rad}} \equiv \omega \times U/S$, where ω is the resonant frequency, U is the electromagnetic energy confined inside the cavity, and S is the Poynting flux radiating out from the cavity. Q_{rad} scales with the particle size as $Q_{\mathrm{rad}} \propto R^{-(2l+1)}$ in the limit of small particle sizes, where l represents the angular momentum of the electromagnetic mode. This scaling rule of Q_{rad} can be understood as the following: If we assume that the electric field remains the same at the cavity boundary $\vec{E}(\vec{r}) \to \vec{E}(\alpha\vec{r})$, as the radius increases from R to αR, then the confined energy is proportional to the cavity volume $U \propto \alpha^3$. On the other hand, the radiated field outside of the cavity is expressed as $E_\theta = \vec{\theta}\cdot\vec{E} = C\frac{1}{r}\frac{d}{dr}[rh_l^{(1)}(k_0 r)]$, where $h_l^{(1)}$ is the spherical Hankel function and C is a prefactor. E_θ asymptotically behaves as $E_\theta \propto Cr^{-l-2}$ when $R \ll \lambda$. Since E_θ is required to be continuous at the cavity boundary, C scales as $\alpha^{l+2}C$ as R becomes αR. The Poynting flux S is proportional to $|C|^2$. The radiative quality factor $Q_{\mathrm{rad}} \equiv \omega \times U/S$ is therefore proportional to $\alpha^{-(2l+1)}$. From the Mie solution, we calculate the electromagnetic energy confined by the cavity as well as the radiative loss from it. Figure 2(b) shows the calculated result of Q_{rad} versus the particle radius R for a hyperbolic cavity with five functional pairs. We find that the Q_{rad} for the spherical cavities is higher than that from the previously reported rectangular cavities [19].

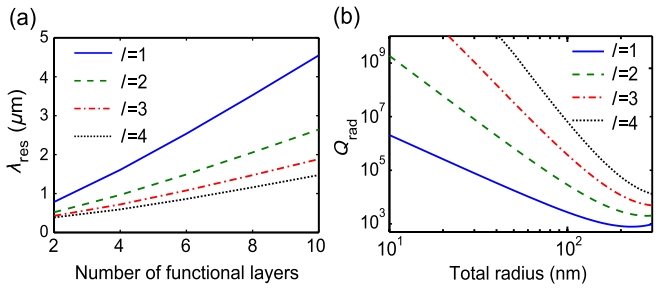

FIG. 2. (a) The maximum resonant wavelength that can be supported by a hyperbolic spherical cavity with an increasing number of functional pairs. The radius of the cavity is fixed to be 100 nm. l represents the angular momentum of the electromagnetic mode. (b) Q_{rad} versus the cavity radius with a different angular momentum l of the electromagnetic resonance. The cavity has five functional pairs.

It is commonly believed that the total quality factor of a LSPP resonator is limited by the intrinsic Ohmic loss. In the electrostatic limit, in which the resonator size is much smaller than the driving wavelength, it has been shown that the resistive quality factor is given by $Q_{\mathrm{static}} = (\omega/2\epsilon_m''(\omega))(d\epsilon_m'(\omega)/d\omega)$, where $\epsilon_m = \epsilon_m' + i\epsilon_m''$ is the permittivity of the metal forming the resonator [15]. Q_{static} depends only on the resonant frequency rather than the geometry of the resonator. As the dimension of the resonator scales up, one introduces more radiative loss and lower Q_{rad}. As a result, the total Q given by $1/Q = 1/Q_{\mathrm{ohm}} + 1/Q_{\mathrm{rad}}$ is further decreased. Overall, the quality factor of a subwavelength plasmonic resonator is typically limited by the electrostatic value. In this hyperbolic spherical cavity case, however, the electromagnetic wave can still be confined in a subwavelength region, while the Q factor exceeds the value predicted in the electrostatic limit. Figure 3(a) shows the total Q as well as Q_{ohm} as functions of particle size, taking the quadrupolar resonance ($l = 2$) in a cavity with five functional pairs as an example. The quality factor of the resonator is calculated according to $Q = \omega'/2\omega''$, where $\omega = \omega' - i\omega''$ is the eigenfrequency calculated using the Mie solution, taking into account the dispersion of the metal. The Q_{ohm} is calculated using $Q_{\mathrm{ohm}} = \omega' U/\gamma_{\mathrm{ohm}}$, where U is the confined energy and γ_{ohm} is the energy-dissipation rate due to the Ohmic loss. Because Q_{rad} is orders of magnitude higher than Q_{ohm}, the Q factor is essentially defined by Q_{ohm}. When $R \to 0$, Q indeed conforms to the predicted electrostatic value $Q_{\mathrm{static}} \approx 54$. As the radius of the cavity increases to 600 nm, which is still subwavelength compared to the resonant wavelength of 2.6 μm, both Q and Q_{ohm} exceed the electrostatic limit by a factor of 2.

Here, we explain that the increased Q factor compared to the electrostatic limit is due to the electrodynamical confinement of the fields. In Fig. 3(b), we decompose the confined electromagnetic energy into three parts: the electric energy in metal $U_E^{(m)}$, the electric energy in dielectric $U_E^{(d)}$, and the total magnetic energy U_H. In the limit of a small cavity size, all of the energy is stored in the

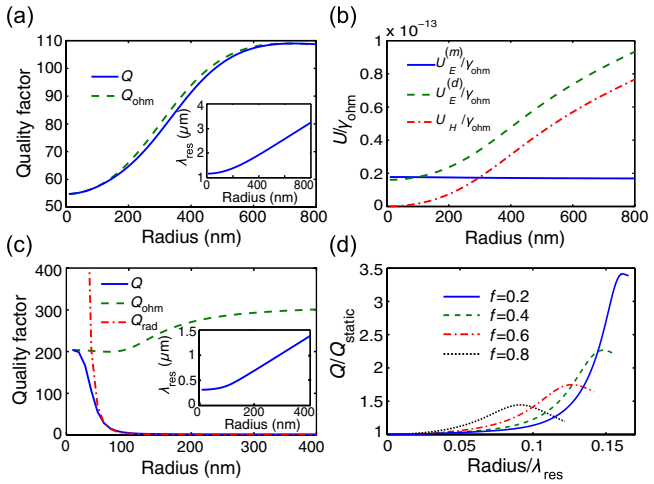

FIG. 3. (a) Q (solid line) and Q_{ohm} (dashed line) of a quadrupolar resonance ($l = 2$) supported by a hyperbolic cavity with five functional pairs. The inset shows the resonant wavelength as the cavity radius R increases. (b) Distribution of the electromagnetic energy divided by the Ohmic damping as the cavity radius R increases. Electric energy in metal $U_E^{(m)}$, electric energy in dielectric $U_E^{(d)}$, and magnetic energy U_H are calculated from the quadrupolar eigenmode supported by a cavity with five functional pairs. (c) Q, Q_{ohm}, and Q_{rad} are calculated from the quadrupolar eigenmode supported by a solid silver nanoparticle. The inset shows the resonant wavelength as the particle radius increases. (d) Enhancement factors compared with the electrostatic limit (Q/Q_{static}) with different filling ratios of the hyperbolic medium. The Q factors are calculated from dipolar eigenmodes supported by cavities with five functional pairs.

form of electric energy. In addition, the electric energy inside the dielectric region is less than that in the metallic region, which is consistent with the electrostatic prediction [15]. As the particle size increases, the energy stored in the magnetic field increases significantly, representing the electrodynamical behavior of the confined fields. Moreover, the electric energy stored in the dielectric part, which does not contribute to Ohmic loss, can actually become more than that in the metal. The increased portion of both U_H and $U_E^{(d)}$ results in a higher Q factor of the resonant modes, as these components are not associated with resistive damping inside metal.

For the enhanced total Q to be observed, it is important that Q_{rad} remain larger than Q_{ohm} when the particle size increases and the resonance becomes electrodynamic. Otherwise, the radiative damping will dominate the dissipation process, resulting in a smaller Q factor, as is typically found in LSPP resonators. Figure 3(c) shows an example of the quadrupolar resonance from a simple spherical nanoparticle made of silver. First of all, we see that Q_{ohm} only increases by 50% as the radius increases to 400 nm. More importantly, the radiative damping dominates over the resistive damping when the particle size increases, as can be seen from the rapidly decreasing Q_{rad} in Fig. 3(c). As a result, the total Q factor decreases monotonically with increasing particle size. We should note here that the large Q factor of the nanoparticle ($Q \approx 200$) in the electrostatic limit is due to the underestimated Ohmic loss in the Drude-model permittivity we use for silver. The fitting parameters in the Drude model are appropriate in the near-infrared to midinfrared frequency range, but not for the visible frequency range.

We find that the maximum enhancement of the Q factor strongly depends on the filling ratio of the metal f. Smaller f results in a higher Q factor, which is intuitive because a smaller metallic region will generate less Ohmic dissipation. Figure 3(d) shows Q/Q_{static} from the dipolar resonances as a function of R/λ_{res} for various filling ratios, with λ_{res} being the resonant wavelength. As f decreases from 0.8 to 0.2, the maximum Q/Q_{static} increases from 1.5 to 3.5. Increasing the number of layers also enhances the maximum Q/Q_{static}, but not as significantly as changing f.

As a result of confining electromagnetic waves inside a small hyperbolic cavity with WGMs, the photonic local density of states (LDOS) can be greatly enhanced. The enhancement of the LDOS inside a cavity (LDOS_c) compared to that in a homogeneous medium (LDOS_0) is defined as the Purcell factor $f_P \equiv \mathrm{LDOS}_c/\mathrm{LDOS}_0$. The Purcell factor is often expressed in terms of the Q factor and the mode volume V_{mode}, according to $f_P = \frac{3}{4\pi^2}(\lambda/n)^3(Q/V_{\mathrm{mode}})$, where λ is the resonant wavelength and n is the local optical index. However, it has been pointed out that the definition of f_P using Q and V_{mode} is not appropriate for subwavelength plasmonic resonators [23], mainly because V_{mode} is not well defined, and also multiple resonances could possibly overlap. Here, we use the dyadic Green's function to calculate LDOS_c directly [24] and then compare to $\mathrm{LDOS}_0 = n^3\omega^2/\pi^2c^3$ in the homogeneous medium to obtain f_P. A spherical wave expression for the dyadic Green's function inside a homogeneous medium can be found, for example, in Ref. [22]. The Green's function with the source inside the hyperbolic cavity is obtained by including the scattered fields from the interfaces of the multilayer structure [22]. Figure 4(a) shows f_P as a function of position calculated from a cavity with a 100-nm radius and five functional pairs. A f_P of more than 10^5 can be obtained inside the dielectric region of the hyperbolic cavity. The strongly enhanced f_P is mainly due to the large λ_{res}-to-radius ratio. In Fig. 4(b), we compare the WGMs of different angular momenta inside cavities made of increasing numbers of functional pairs. The dipolar resonance has the largest f_P because its resonant wavelength is the longest. Also, f_P becomes larger as the number of functional pairs increases. Finally, we find that f_P is roughly proportional to R^{-3} in the limit of small cavity sizes, as is shown in Fig. 4(c).

In the case of translationally invariant HMMs, it has been suggested that the divergence of the LDOS can occur because of the infinite number of propagating modes

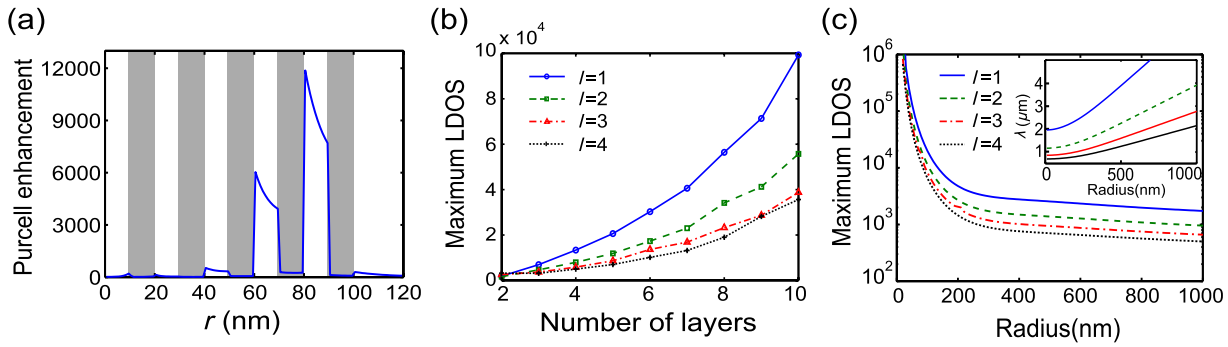

FIG. 4. (a) Enhancement of the LDOS as a function of position r calculated at the wavelength of the quadrupolar resonance ($l = 2$). The hyperbolic cavity is made of five functional pairs and has a total radius of 100 nm. The grey areas indicate the metallic regions. (b) The maximum LDOS enhancement taken over the cavity volume versus the number of functional pairs. The radius of the cavity is fixed as 100 nm. l represents the angular momentum. (c) The maximum LDOS enhancement with decreasing cavity radius. The number of functional pairs is fixed as 5. The resonant wavelengths corresponding to the WGMs in (b) are plotted in Fig. 2(a), while the resonant wavelengths in (c) are shown in the inset.

associated with the open hyperbolic isofrequency contour [25]. In a realistic implementation of HMMs using metal and dielectric composites, such a divergence is prevented by several factors [26]: (1) The finite period d of the metamaterial introduces a cutoff in the achievable wave vector and therefore limits the LDOS by $(\lambda/d)^3$ [27]. (2) The spatial dispersion of the metal permittivity regularizes the divergence even in the limit of small d [28]. (3) The finite size a of an emitting dipole placed in a homogeneous HMM limits the LDOS by $(\lambda/a)^3$ [29]. In contrast with the bulk HMMs that have an infinite number of propagating modes with arbitrarily large wave vectors, the LDOS enhancement in the HMM cavities studied here mostly comes from individual WGMs at the resonant frequencies. The LDOS enhancement for the HMM cavities is therefore not limited by $(\lambda/a)^3$ or $(\lambda/d)^3$ but instead by the cavity size and the Ohmic damping rate.

Although the proposed hyperbolic cavities composed of multiple metal-dielectric bilayers seem complicated, the fabrication can potentially be achieved using chemical synthesis approaches [30]. It is to be expected that larger Ohmic damping can occur in association with the quality of the synthesized metal, and the damping rate ω_c that we use in the Drude model needs to be increased accordingly. The increased damping rate will result in a lower Q factor than what we predict in Fig. 3(a). However, the enhancement over the electrostatic Q factor shown in Fig. 3(d) remains the same. In addition to spherical cavities, one may also consider a disk consisting of multiple metal-dielectric rings. Such a hyperbolic disk resonator also supports WGMs in analogy to to the microring resonators but with a much smaller cavity size. The indefinite disk cavity can be coupled to gain media, such as dye molecules, quantum dots, and quantum wells, in order to achieve plasmonic nanolasers in near-infrared and midinfrared frequency ranges. Also, the 2D geometry of the disk resonator makes it easier to be coupled with on-chip waveguides, while the strong near-field enhancement and enhanced Q factor can be useful for applications such as surface-enhanced absorption spectroscopy.

In summary, we show that the hyperbolic cavities composed of alternating metal and dielectric layers can support WGMs. Unlike the dielectric microcavities, the hyperbolic cavities have no lower bound on the geometry dimension and can be made very small while still supporting the WGMs. By confining light in a deep subwavelength region in this type of cavity, the LDOS can be dramatically increased. In addition, we demonstrate that the subwavelength hyperbolic cavities can confine fields in an electrodynamical way, which reduces the Ohmic dissipation and leads to higher-quality factors compared to electrostatic resonances. We should note that there is still a tradeoff between high LDOS and small Ohmic loss. For the hyperbolic cavity studied here, small cavity size benefits the high LDOS since the LDOS is inversely proportional to the cavity size. However, the effect of electrodynamical light confinement is demonstrated when the cavity size is slightly increased. It should be possible to design even smaller cavities with more efficient electrodynamical light confinement. The advantages of reduced Ohmic loss and strong light-matter interaction induced by the extremely high LDOS are advantageous in the applications of nanolasers, quantum optics, nonlinear optics, and so on.

This work was supported by the U.S. Department of Energy, Basic Energy Sciences Energy Frontier Research Center (DoE-LMI-EFRC) under Award No. DE-AC02-05CH11231.

[1] M. S. Tame, K. R. McEnery, Ş. K. Özdemir, J. Lee, S. A. Maier, and M. S. Kim, *Quantum Plasmonics*, Nat. Phys. **9**, 329 (2013).

[2] M. Kauranen and A. V. Zayats, *Nonlinear Plasmonics*, Nat. Photonics **6**, 737 (2012).

[3] D. Englund, D. Fattal, E. Waks, G. Solomon, B. Zhang, T. Nakaoka, Y. Arakawa, Y. Yamamoto, and J. Vuckovic, *Controlling the Spontaneous Emission Rate of Single Quantum Dots in a Two-Dimensional Photonic Crystal*, Phys. Rev. Lett. **95**, 013904 (2005).

[4] V. S. C. Manga Rao and S. Hughes, *Single Quantum-Dot Purcell Factor and Beta Factor in a Photonic Crystal Waveguide*, Phys. Rev. B **75**, 205437 (2007).

[5] A. Kinkhabwala, Z. Yu, S. Fan, Y. Avlasevich, K. Mullen, and W. E. Moerner, *Large Single-Molecule Fluorescence Enhancements Produced by a Bowtie Nanoantenna*, Nat. Photonics **3**, 654 (2009).

[6] K. J. Russell, T.-L. Liu, S. Cui, and E. L. Hu, *Large Spontaneous Emission Enhancement in Plasmonic Nanocavities*, Nat. Photonics **6**, 459 (2012).

[7] D. Pacifici, H. J. Lezec, and H. A. Atwater, *All-Optical Modulation by Plasmonic Excitation of CdSe Quantum Dots*, Nat. Photonics **1**, 402 (2007).

[8] C. Husko, A. De Rossi, S. Combri, Q. V. Tran, F. Raineri, and C. W. Wong, *Ultrafast All-Optical Modulation in GaAs Photonic Crystal Cavities*, Appl. Phys. Lett. **94**, 021111 (2009).

[9] J. Homola, S. S. Yee, and G. Gauglitz, *Surface Plasmon Resonance Sensors: Review*, Sens. Actuators B **54**, 3 (1999).

[10] H. A. Atwater and A. Polman, *Plasmonics for Improved Photovoltaic Devices*, Nat. Mater. **9**, 205 (2010).

[11] Z. Yu, A. Raman, and S. Fan, *Fundamental Limit of Nanophotonic Light Trapping in Solar Cells*, Proc. Natl. Acad. Sci. U.S.A. **107**, 17 491 (2010).

[12] K. A. Willets and R. P. Van Duyne, *Localized Surface Plasmon Resonance Spectroscopy and Sensing*, Annu. Rev. Phys. Chem. **58**, 267 (2007).

[13] P. K. Jain, X. Huang, I. H. El-Sayed, and M. A. El-Sayed, *Noble Metals on the Nanoscale: Optical and Photothermal Properties and Some Applications in Imaging, Sensing, Biology, and Medicine*, Acc. Chem. Res. **41**, 1578 (2008).

[14] E. J. R. Vesseur, F. J. García de Abajo, and A. Polman, *Broadband Purcell Enhancement in Plasmonic Ring Cavities*, Phys. Rev. B **82**, 165419 (2010).

[15] F. Wang and Y. R. Shen, *General Properties of Local Plasmons in Metal Nanostructures*, Phys. Rev. Lett. **97**, 206806 (2006).

[16] S. L. McCall, A. F. J. Levi, R. E. Slusher, S. J. Pearton, and R. A. Logan, *Whispering-Gallery Mode Microdisk Lasers*, Appl. Phys. Lett. **60**, 289 (1992).

[17] H. Lee, T. Chen, J. Li, K. Y. Yang, S. Jeon, O. Painter, and K. J. Vahala, *Chemically Etched Ultrahigh-Q Wedge-Resonator on a Silicon Chip*, Nat. Photonics **6**, 369 (2012).

[18] D. R. Smith and D. Schurig, *Electromagnetic Wave Propagation in Media with Indefinite Permittivity and Permeability Tensors*, Phys. Rev. Lett. **90**, 077405 (2003).

[19] X. Yang, J. Yao, J. Rho, X. Yin, and X. Zhang, *Experimental Realization of Three-Dimensional Indefinite Cavities at the Nanoscale with Anomalous Scaling Laws*, Nat. Photonics **6**, 450 (2012).

[20] P. B. Johnson and R. W. Christy, *Optical Constants of the Noble Metals*, Phys. Rev. B **6**, 4370 (1972).

[21] C. F. Bohren and D. R. Huffman, *Absorption and Scattering of Light by Small Particles* (Wiley, New York, 1998).

[22] A. Narayanaswamy and G. Chen, *Thermal Near-Field Radiative Transfer between Two Spheres*, Phys. Rev. B **77**, 075125 (2008).

[23] A. F. Koenderink, *On the Use of Purcell Factors for Plasmon Antennas*, Opt. Lett. **35**, 4208 (2010).

[24] G. Colas des Francs, C. Girard, J.-C. Weeber, C. Chicane, T. David, A. Dereux, and D. Peyrade, *Optical Analogy to Electronic Quantum Corrals*, Phys. Rev. Lett. **86**, 4950 (2001).

[25] Z. Jacob, I. I. Smolyaninov, and E. E. Narimanov, *Broadband Purcell Effect: Radiative Decay Engineering with Metamaterials*, Appl. Phys. Lett. **100**, 181105 (2012).

[26] A. Poddubny, I. Iorsh, P. Belov, and Y. Kivshar, *Hyperbolic Metamaterials*, Nat. Photonics **7**, 948 (2013).

[27] O. Kidwai, S. V. Zhukovsky, and J. E. Sipe, *Dipole Radiation near Hyperbolic Metamaterials: Applicability of Effective-Medium Approximation*, Opt. Lett. **36**, 2530 (2011).

[28] W. Yan, M. Wubs, and N. A. Mortensen, *Hyperbolic Metamaterials: Nonlocal Response Regularizes Broadband Supersingularity*, Phys. Rev. B **86**, 205429 (2012).

[29] A. N. Poddubny, P. A. Belov, and Y. S. Kivshar, *Spontaneous Radiation of a Finite-Size Dipole Emitter in Hyperbolic Media*, Phys. Rev. A **84**, 023807 (2011).

[30] E. Prodan, C. Radloff, N. J. Halas, and P. Nordlander, *A Hybridization Model for the Plasmon Response of Complex Nanostructures*, Science **302**, 419 (2003).